15

Prototype of a hybrid muon tomograph for muonography of large-scale objects

© N.A. Pasyuk,[1] N.N. Davidenko,[2] A.S. Kozhin,[1,3] K.G. Kompaniets,[1] Yu.N. Konev,[2] S.V. Oleinik,[2] A.A. Petrukhin,[1] R.M. Fakhrutdinov,[1,3] M.Yu. Tselinenko,[1] D.V. Shudra,[2] V.V. Shutenko,[1] I.I. Yashin[1]

[1] National Research Nuclear University „MEPhI“,
115409 Moscow, Russia
[2] All-Russian Research Institute for the Operation of Nuclear Power Plants 109507 Moscow, Russia
[3] A.A. Logunov Institute for High Energy Physics of the National Research Center „Kurchatov Institute“,
142281 Protvino, Moscow Region, Russia
e-mail: NAPasyuk@mephi.ru

Received February 15, 2024
Revised May 30, 2024
Accepted May 31, 2024

A fully functional prototype, consisting of the same components, was assembled at the MEPhI to test the muonography technology before assembling the final version of the muon tomograph. An experiment on spatial localization of test objects assembled from lead bricks using the muonography method was carried out to test the performance of the developed hardware-software complex and data processing methods. The article describes the design of a prototype hybrid muon tomograph, the applied techniques for reconstructing events and constructing muonograms, and also presents the main results of experiments on the localization of lead assemblies in space based on the analysis of difference muonograms.

Keywords: cosmic ray muons, particle detectors, scintillation strips, SiPM, scintillation detector, drift tube, muon hodoscope, muonography, muon tomography, muonogram.

DOI: 10.61011/TP.2024.08.59019.40-24

Introduction

Presently, a new direction of experimental physics has gained a strong momentum — muonography of large-scale objects of natural and artificial origin using muons — a penetrating component of secondary cosmic rays. The intensity of muons on the Earth's surface is about $100\,\mathrm{m}^{-2}\cdot\mathrm{s}^{-1}$. The muon flux is formed at altitudes of $15-20$ km mainly in the decays of charged π- and K-mesons produced by the interaction of protons and nuclei of primary cosmic rays with the nuclei of atmospheric atoms.

Muons in the process of passing through matter lose energy mainly to ionization and radiation processes, and also experience multiple Coulomb scattering on nuclei, which results in a change of the particle flow. The high penetrating power makes cosmic muons an attractive source for remote sensing of the structure of large-scale objects. The average energy of muons on the Earth's surface coming from the vertical direction is about 4 GeV, which allows them to pass through ~ 20 m of water. The angular distribution of the muon flux depends on the zenith angle measured from the vertical, as $\sim \cos^2(\theta)$, and the average energy increases as $\sim \sec(\theta)$.

2D-matrix — muonographs — density distribution of the intersection points of the tracks with the plane can be obtained (by analogy with an X-ray pattern) by projecting muon tracks recorded by a hodoscope in the direction of some reference plane passing through the center of the „illuminated“ object. The obtained muonographs of the object with several hodoscopes from different intersecting directions provide the opportunity for a 3D-analysis (tomography) of the structure of the object [1–3]. The use of a single hodoscope that moves around the studied object is another method of implementation of the muon tomography.

A mobile hybrid muon hodoscope was created in Scientific & Educational Centre NEVOD (National Research Nuclear University MEPhI) in cooperation with JSC „VNIIAES“ (Rosatom) under the order of JSC „Science and Innovation“ (Rosatom Group) for the implementation of the muonography method [4] for the remote diagnostics of large-scale objects, including nuclear reactors. The hodoscope has a modular design and consists of two hodoscopic systems [5–8]: scintillation strip detector (SSD) and drift tube detector (DTD). Each of the detectors is a system of single-projection coordinate planes (SCP) arranged sequentially with orthogonally oriented strips (tubes) and forming a two-coordinate registration system that ensuring the independent detection of muon tracks in the form of vertical and horizontal projections. Each SSD single-projection plane consists of two adjacent modules of 64 narrow and long scintillation strips with fiber-optic light collection on silicon photomultipliers (SiPM). The DTD single-projection plane consists of two assembly chambers with three layers of 48 drift tubes each (a total of 288 tubes).

Each detector has its own advantages: the strip detector has a high speed, forms a trigger and determines the initial position of the track, and the drift tube detector has a high coordinate resolution and makes it possible to

form muonographs with a resolution second only to nuclear emulsions.

A fully functional prototype of a hybrid muon hodoscope (HMH) was assembled and tested to verify the developed design solutions of the recording system, as well as to develop methods for reconstructing events and evaluating the possibility of constructing muonographs of large-scale objects.

A suspended temporary structure of the HMH prototype incorporating SSD, DTD, trigger system, data collection and processing systems was mounted in a special hangar-type building. Experiments were conducted using the HMH prototype to check the performance of the main systems and data reconstruction, processing and analysis methods used for constructing muonographs. The main objective of the experiments was to detect and evaluate the accuracy of localization of test objects (assemblies of standard lead bricks) by muonography at various distances and heights from the center of the HMH prototype.

This paper describes the design and characteristics of the HMH prototype, discusses the features and basic principles of the developed methods for reconstructing events and constructing muonographs, as well as the first results of muonography of lead blocks using the HMH prototype.

1. Design of the hybrid muon hodoscope prototype

The HMH prototype has a modular structure design and consists of two hodoscopes, a scintillation strip detector and a drift tube detector. The SCP of the detectors alternate with each other (Fig. 1) and are fixed in a vertical position on suspensions to a ceiling beam (Fig. 2). Each plane is additionally fixed to a special frame on the floor to eliminate the possibility of rotation. The coordinate planes of the SSD in the prototype version of the HMH represent only one module (64 strips). The SCP with horizontally oriented strips are placed at different heights to ensure the best capture of the flux of single muons at the zenith angle of $\sim 70^\circ$. The distance between the extreme planes is ~ 3.5 m in the assembled structure with the use of 6 SSD SCP (384 scintillation strips) and 4 DTD SCP (1152 drift tubes).

1.1. Scintillation strip detector

The SSD is a multichannel detection system consisting of six SCP [9]. Each SCP used in experiments with the HMH prototype is formed from one basic module (BM) in size (L×W×T) $3196 \times 1500 \times 57$ mm with sensitive area of 2960×1478 mm^2. The BM consists of 64 sequentially stacked scintillation strips manufactured by LLC „Uniplast“ (Vladimir) [10], the light is collected along the length of which is carried out using an glued spectrum-shifting fiber (Wave Length Shifter) KURARAY Y-11(200)SJ [11]. The signal is registered from light-absorbing fibers by SiPM Hamamatsu S13360-1350CS [12]. The strip is made using

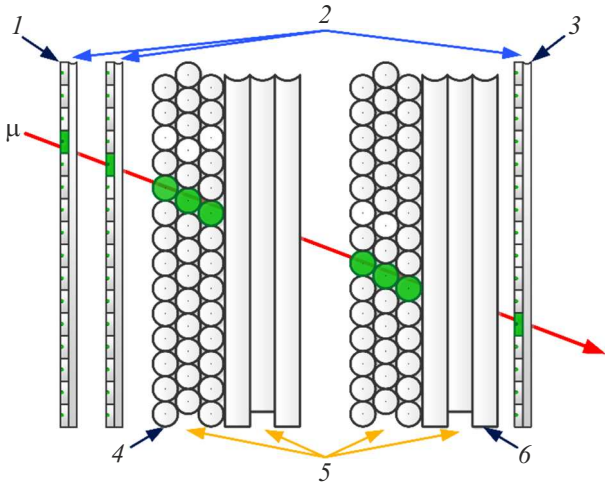

Figure 1. Layout of the detecting elements of the HMH prototype: *1* — „X“ strips, *2* — planes with scintillation strips, *3* — „Y“ strips, *4* — „X“ tubes, *5* — planes of chambers with drift tubes, *6* — „Y“ tubes.

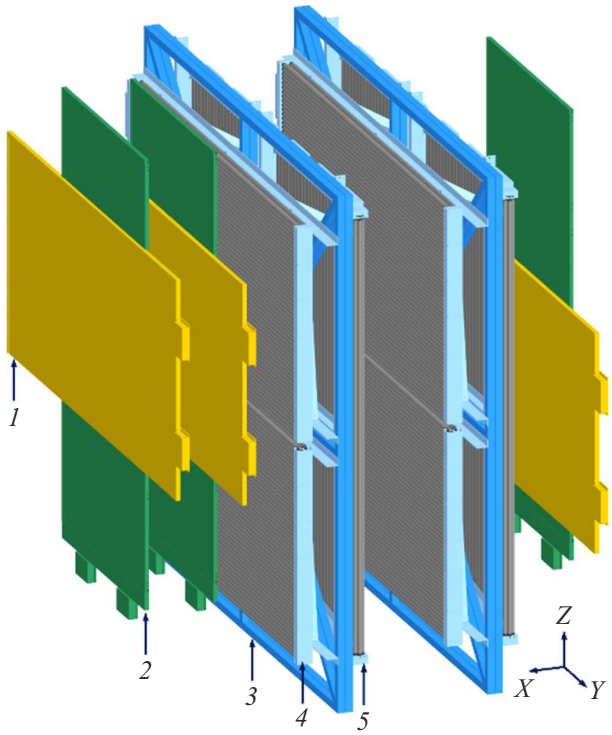

Figure 2. 3*D*-model of HMH prototype: *1* — SSD plane with horizontal strips, *2* — SSD plane with vertical strips, *3* — bearing frame of the DTD module, *4* — DTD plane with horizontal tubes, *5* — DTD plane with vertical tubes.

the technology of extrusion of scintillator sheet blanks in the form of a strip with a size of $2960 \times 23 \times 7$ mm. The outer surface of each strip is covered with a thin layer of foamed polystyrene having a high diffuse light reflection coefficient. A spectrum-containing fiber with a diameter of 1 mm is glued into the groove in the middle of one of the wide

faces of the strip to re-emit photons from the blue part of the visible light spectrum into green. Photons at the fiber output are registered by SiPM via an optical connector glued into the strip [9].

The SSD is an independent registration system. Signals from SiPM of a single BM are processed by two readout electronics boards based on the 32-channel chip ASIC Petiroc 2A [13] paired with FPGA Altera Cyclone III EP3C16Q240C8N. All BM are synchronized through the triggering control central unit (CU) [9] based on Altera DEO-NANO-SoC FPGA Cyclone V [14] with adapter boards for the possibility of connecting a large number of readout boards. At a given multiplicity of incoming signals from triggered planes, the CU generates a signal about data storage in the LVDS standard and sends it to all FPGA boards of the BM, as well as to the DTD readout electronics, where this label serves as a synchronization point for two detectors. At the same time, data from all triggered channels is read and transmitted by the data acquisition system to the central computer via Ethernet. The settings of the ASIC chip, the SiPM supply voltage unit, and data exchange with interface chips are controlled using FPGA in addition to formation of an internal trigger condition.

1.2. DTD

The DTD is a multichannel detection system consisting of four SCP [15]. Each SCP is formed from two chambers consisting of drift tubes. Each drift tube chamber with the size of (D×T×D) $3520 \times 1460 \times 210$ mm and sensitive area of 2960×1453 mm is mounted on a duralumin frame and comprises an assembly of 144 drift tubes glued into three parallel layers of 48 tubes and connected to a data acquisition system [16]. The middle row of tubes is offset by half the diameter of the tube, the distance between the centers of any two adjacent tubes in the chamber and in the plane is 30 mm. Similar three-layer assemblies of drift tubes are used in the muon detector of the ATLAS facility at the Large Hadron Collider at CERN (Geneva) [17].

The drift tube used in DTD was developed in NRC „Kurchatov Institute“- IHEP (Protvino) and is a thin-walled aluminum cylinder with a wall thickness of 0.40mm, length of 2996mm and an outer diameter of 29.97mm jcite18. A gold-plated signal wire with a diameter of 0.05mm made of tungsten-rhenium alloy ($97\%W + 3\%Re$) is used as the anode. All tubes in each layer of the chamber are connected in sequential chains using gas jumpers. The last tube of the extreme layer of the chamber is connected to a common gas collector, into which a gas mixture Ar-CO_2 is fed through a regulating reducer in the ratio of 93 : 7.

Functionally, each drift tube is an independent recording channel. The MT-48 board is used for data reading which simultaneously registers the signal from 48 tubes. Each drift tube chamber has three independent reading boards MT-48 [16] based on Altera EP1K100QC208 chips. A USB hub is used for interaction with the boards and the general synchronization and reception of the trigger from the SSD is performed via the signal splitter board RMT-48 [16] based on the Altera MAX3000ATX100 chip.

2. Event reconstruction methods

Local and laboratory coordinate systems were set to implement the event reconstruction methods. The use of two coordinate systems makes it easy to take into account the position of detectors in space by moving and rotating the local coordinate system relative to the laboratory coordinate system. The presence of two coordinate systems is also justified by the applied methods of event reconstruction based on projections of particle tracks.

A straight line is first constructed in a local coordinate system for obtaining a projection which is unified in each single-coordinate plane, using in this case only two coordinates instead of three coordinates when using a common (laboratory) coordinate system.

The right rectangular coordinate system was chosen for the laboratory coordinate system (LabCS) [19], the beginning of this coordinate system lies in the corner of the building accommodating the HMH prototype. Strips and tubes in a separate coordinate plane are oriented in a certain direction, coinciding with the direction of either Y_{Lab} (vertical) or Z_{Lab} (horizontal) axes of the laboratory coordinate system linked to the hodoscope. The axis X_{Lab} coincides with the axis of the detector, directed perpendicular to the coordinate planes in the direction of the observed object.

The beginning of the local coordinate system (LocCS) of the SSD is tied to the coordinates of the first strips of the BM SCP, where the axis $X_{\mathrm{loc}}^{\mathrm{SSD}}$ is directed along the strip, $Z_{\mathrm{loc}}^{\mathrm{SSD}}$ is directed along the numbering of the strips in the BM assembly, and $Y_{\mathrm{loc}}^{\mathrm{SSD}}$ is directed towards the upper edge of the strip. The origin of the local coordinate system DTD is linked to the coordinates of the first tubes of the drift chambers, where the axis $X_{\mathrm{loc}}^{\mathrm{DTD}}$ is directed along the tube, $Z_{\mathrm{loc}}^{\mathrm{DTD}}$ is directed along the numbering of the tubes in the layer, and $Y_{\mathrm{loc}}^{\mathrm{DTD}}$ is directed in the direction of the increase of the number a layer of tubes.

Reconstruction of track parameters in detectors is based on its registration by several SCP. Muons cross the detector SCP, which triggers the operation of counters of the recording system. Each coordinate plane provides information about the triggered channels, which allows estimating the coordinate of the point of intersection of the SCP assembly by the muon. The data of several coordinate planes with the corresponding orientation of the strips (tubes) allow the reconstruction of the track in the corresponding projection planes XY and XZ. Information about two projections makes it possible to restore the track in space. The set of reconstructed tracks allows building a shadow image (muonograph) of the studied object in the muon flux.

2.1. Reconstruction of tracks in a strip detector

SSD contains 6 SCP scintillation strips: strips are oriented along the axis Y in three SCP, strips are oriented along the axis Z in LabCS in the other three SCP. In this case, the events are registered by highlighting the interplanar coincidences of signals. Since each projection plane (XY and XZ) contains three layers of strip projections (Fig. 3), the method of searching for combinations of triggered strips lying on straight lines was chosen for the reconstruction of single tracks. The presence of at least three triggered Y-planes and at least three Z-planes at the same time is checked for the track reconstruction, since this makes it possible to effectively distinguish events with single muons from multiparticle events. In this case, the event selection algorithm can be optimized based on the established trigger condition of interplanar coincidences.

Curved particle trajectories are discarded when selecting events based on the assumption that the muon track is straight. The track is searched sequentially for XY- and XZ-projections of the SSD. Fig. 4 shows an illustration of the algorithm for searching a „straight-line“ section using the coordinates of triggered strips in the XY projection plane. The algorithm is based on a sequential search through all triggered strips and searching for all possible „straight-line“ sections. The coordinates of the centers of the triggered strips, for which a straight line is best described, are used for the final reconstruction of the track. The width of the permissible area $w = k23.1$ mm is used as a criterion for finding the triggered strip on the expected „straight-line“ section, where 23.1 mm is the width of the strip plus the distance between two adjacent strips in BM, and k is a

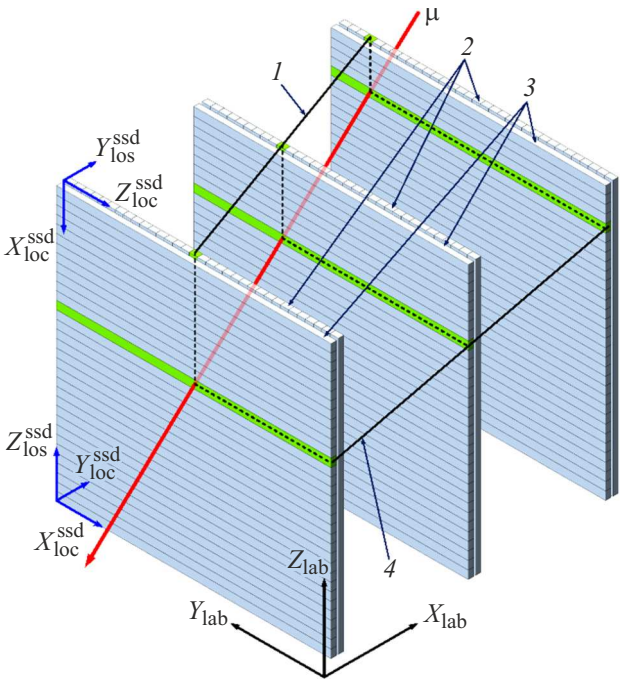

Figure 3. Finding track projections in SSD: *1* — XY-projection, *2* — Z-plane, *3* — Y-plane; *4* — XZ-projection.

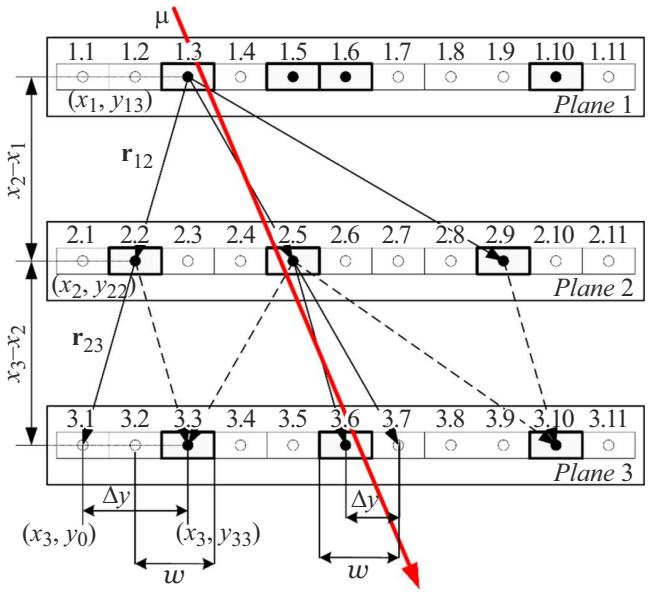

Figure 4. Illustration of the algorithm for searching „straight-line“ section in the XY projection.

number indicating the number of strips included in the permissible search area for triggered strips in SCP.

The search starts from the upper (initial) triggered plane in the illustration of the algorithm shown in Fig. 4. The points of the intersecting line in each plane are numbered consecutively from the lowest numbers of the centers of the triggered strips to the highest ones.

An array of triggered points $(i,\ j)$ is considered, where j is the number of the triggered point in the plane number i. The coordinate of the center of the first triggered strip in the row is taken (in this case 1.3) for the case shown in Fig. 4 and is connected by a straight line to the first point (the center of the first triggered strip) on the adjacent plane (2.2). Then the line continues from the point (2.2) and the point of intersection of this line y_0 with the line passing through the centers of the strips is sought. Also, a line is drawn from the point (2.2) to the center of the first triggered strip of the next plane (3.3). The difference Δy between y-coordinate of the middle of the next checked triggered strip (3.3) and the y_0 of the tested plane x_3 is used to check the „straightness“ $\Delta y = y_{33} - y_0$. The next point on the same plane is taken if the point does not belong to a permissible area (the condition $|\Delta y| > w$ will be met). Since the viewing of points in the plane goes in the direction of the increase of y, if the value of Δy in the next plane is positive and already exceeds w, a return to the previous plane occurs and a test line from another point is built, followed by searching through new points. The points are enumerated until $|\Delta y|$ becomes less than or equal to w (the condition $|\Delta y| \le w$ will be met). This is a straight line between the points $1.3 \to 2.5 \to 3.6$ for the example shown in Fig. 4. The following parameters are recorded for this section:

— average value Δy: $\langle \Delta y \rangle$;
— module of the average value Δy: $|\langle \Delta y \rangle|$;
— numbers of points belonging to the found straight-line section.

Similarly, the search for other „straight-line“ sections is carried out and their characteristics are recorded both in the current and in other combinations of triggered planes. The sites with a lower value of the parameter $Crit = |\Delta y/3|$ are selected from all sections found. Then the following procedures are carried out sequentially:
— linear approximation of selected candidate points;
— search for points in a corridor with a width of L;
— the final linear approximation of all points inside the corridor of $L = 40$ mm.

The described procedure is performed for Y- and Z-strips independently (for the XY- and XZ-projections of SSD). Next, a tack is found in space according to the received projections of the track. The particle track (straight line) obtained in this manner is then used to analyze angular distributions and construct muonographs.

2.2. Reconstruction of tracks in drift detector

Information about the coordinates of the centers of the triggered tubes (anode wires) and their trigger times is used to reconstruct events in the DTD.

Events are registered continuously during consecutive intervals („windows“) with a duration of 16.8 ms. In this case, the time of occurrence of the pulse is recorded with a discreteness of 1 ns relative to the beginning of the „window“ registration. A clustering procedure is performed to separate muons into single particles since several muons can pass through the detector in the interval of the „window“The clustering process consists of searching for consecutive groups (clusters) of triggered tubes for which the difference in triggering times does not exceed 800 ns (maximum drift time). The condition of the presence of signals from at least 11 tubes in all four single-projection coordinate planes is used as a criterion for the passage of a single particle through DTD, and there should be at least two triggered tubes in each plane of the detector. Figure 5 shows an example of clustering of events in the „window“ by time for one drift tube chamber, the tube triggering times is shown by the color gradation.

The reconstruction of track segments in the chambers in which clusters are detected is carried out if the condition of „at least 11 tubes“ in the detector is met. Each three-layer chamber on drift tubes allows obtaining only a projection of a track segment in the corresponding coordinate plane: XY or XZ.

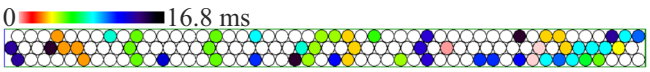

Figure 5. Clustering of events by time within a single dataset „window“.

The reconstruction of the track segment is based on an estimate of the distances from the centers of the anode wires to the track that passed through them by the relative times of their operation. This is done using the $r(t)$-dependence, which is obtained from the calibration results based on the clustering procedure for all events in the window 168 s. Relative triggering times are calculated for tubes of each cluster. To do this, the minimum time t_0 is subtracted from the cluster tube triggering time. At the same time, the relative triggering time of each tube in the cluster is systematically shifted towards shorter times. Then, the total time spectrum is plotted for all clusters selected in the time window (Fig. 6). The zero bin is removed from the obtained distribution and integration is performed with respect to the radius of the tube. The resulting curve (Fig. 7) represents the desired $r(t)$-dependence for one tube. This dependence relates the triggering time relative to t_0 for the cluster in

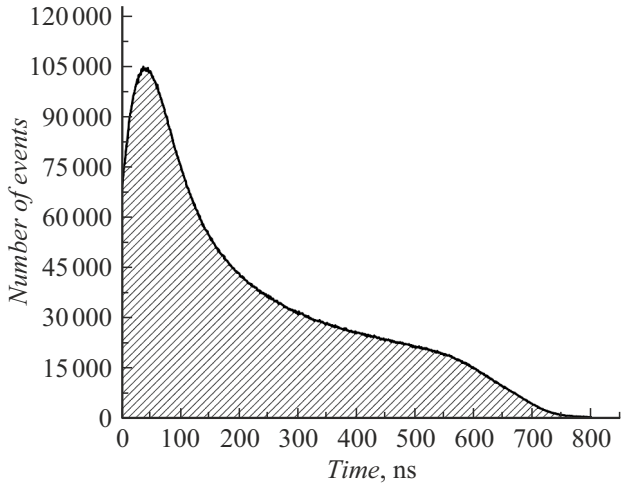

Figure 6. Time spectrum of clustered signals.

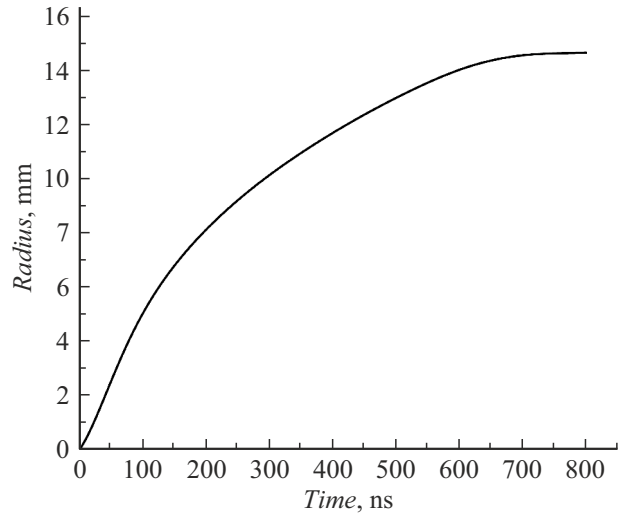

Figure 7. Dependence $r(t)$ obtained from the time spectrum integral.

which the tube is located, and the distance from the wire of this tube to the particle track.

After identification of groups (clusters) of triggered tubes, track projections are found that could give the observed combination of triggered tubes in the group.

The algorithm is based on the Hough Transform method [20]. Figure 8 shows the local and laboratory coordinate systems that are used to reconstruct the track using DTD. The track consists of two segments in each projection, which are represented in parametric form (in the LocCS, the axis Z is directed along the numbering of the tubes, and the axis Y is directed along the numbering of the tube assembly layers):

$$z\sin(\varphi) + y\cos(\varphi) = c. \tag{1}$$

This representation is convenient because it allows for a linear calculation of the distance from the track to an arbitrary point (y_0, z_0), which determines the coordinate of the anode wire of the triggered drift tube in the coordinate system (r, φ):

$$r = c - \sin(\varphi)z_0 - \cos(\varphi)y_0. \tag{2}$$

In this case, the reconstruction task is reduced to finding a tangent that optimally describes the circles in the triggered tubes of the cluster, the radii of which are determined using $r(t)$-dependences. The tangent line $ay + bz + c = 0$ (Fig. 9) can be obtained from the equation (2) by introducing the following notations: $a = \cos(\varphi)$; y — coordinate of the abscissa axis; $b = \sin(\varphi)$; φ — inclination angle of the radius vector; z — coordinate ordinate axis; $c = -r$; r — radius vector.

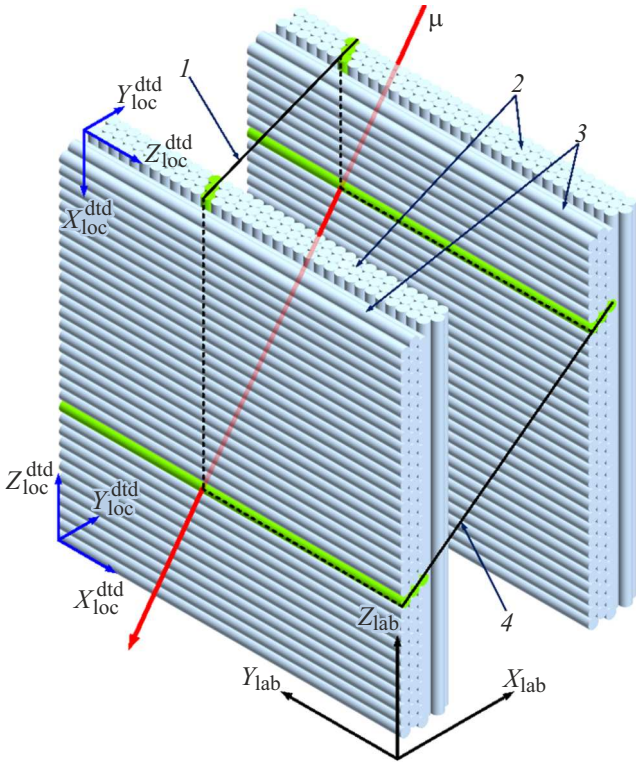

Figure 8. Finding track projections in DTD: *1* — XY-projection; *2* — Z-plane; *3* — Y-plane; *4* — XZ-projection.

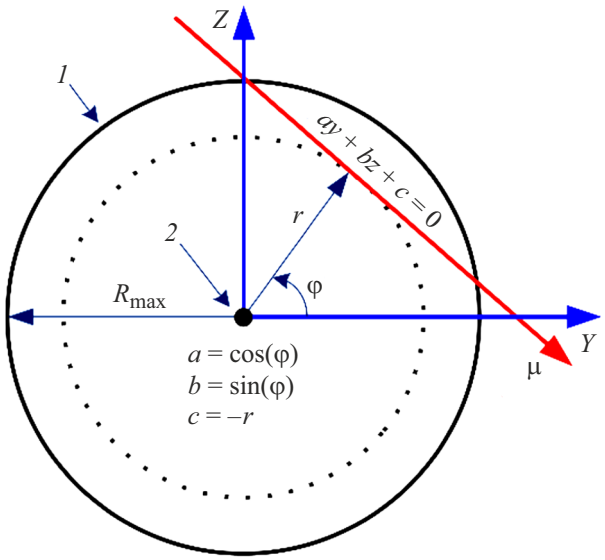

Figure 9. Illustration of the equation of tangent to a circle: *1* — cathode, *2* — anode.

It is easy to see that the distance is determined with a sign, which can be fixed by introducing orientation on the track. From a practical point of view, it is convenient to consider a track propagating in the Y direction. This choice fixes the sign $\sin(\varphi) > 0$.

The track parameters are obtained as a result of minimization of the functional by the least squares method based on the Levenberg–Marquardt algorithm [21]:

$$X^2(a, b, c) = \sum_i^N \frac{(ay_i + bx + c - r_i)^2}{(\sigma_{r_i})^2}, \tag{3}$$

where N — the number of triggered tubes, the value σ_r takes into account the time of signal passage through the wire, the muon time of flight, the intrinsic resolution of the tubes and the contribution of multiple scattering on the detector material.

It is not enough to consider each chamber separately for reconstruction of projections of particle tracks in space, it is necessary to analyze the operation of all projections together. This is due to the fact that the local coordinate system of the SCP can be displaced and rotated by a certain angle both relative to the local coordinate system of another plane with a similar orientation of the chamber, and relative to the LabCS. The values of displacements and rotations are determined by the quality of the mounting of chambers and planes in general, and are carefully measured before taking measurements.

Then, segments are searched in different chambers belonging to the same track projection. Similar segments the angle between which does not exceed $\Delta\varphi = 5°$ are

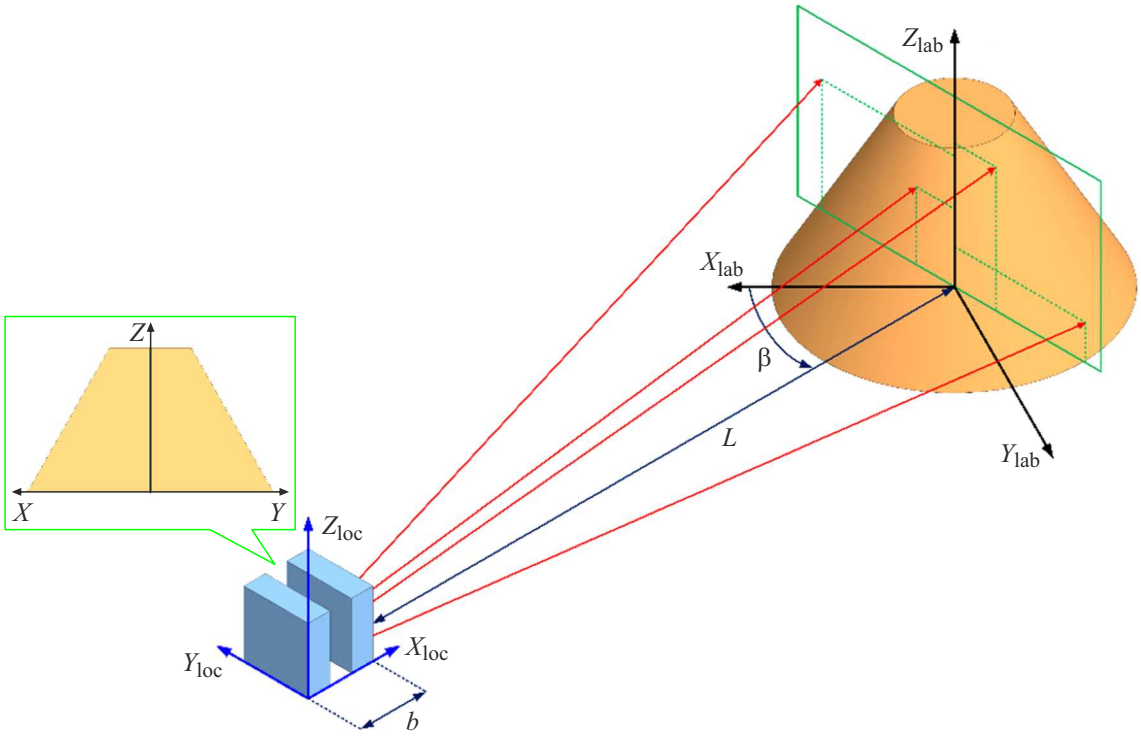

Figure 10. Muonograph construction diagram.

searched for this purpose in each chamber of the same projection using the found straight lines (segments of the particle track). Two segments are linked together. A plane parallel to the direction of the tubes is drawn through each segment of the track for this purpose.

After finding the projection planes of the tracks in separate chambers, it is necessary to compare them to each other for finding a common projection of the track that corresponds to the track of a single particle. It is necessary to find the equation of the common surface (4) to compare the projections since the drift chambers are located at some distance from each other and the orientation of their axes may differ due to installation errors. This can be done using a normal vector to the surface $n = (A, B, C)$:

$$Ax + By + Cz + D = 0, \tag{4}$$

$$A = \frac{V_x}{|V|}; B = \frac{V_y}{V}; C = \frac{V_z}{V}; D = -\frac{(P_1 V)}{|V|}, \tag{5}$$

$$V = (P_2 - P_1) \times (P_3 - P_1), \tag{6}$$

where A, B, C are unit vectors in the corresponding axes, D is the distance from the origin of the coordinate system to the plane in question, P_1 and P_2 are the midpoints of the projection of the first OPC in $X_{\text{Loc}}^{\text{DTD}}$- coordinate of the beginning and end of the working area of the tube, respectively, P_3 and P_4 — the midpoints of the projection of the second SCP in $X_{\text{Loc}}^{\text{DTD}}$-coordinate of the beginning and end of the working zone of the tube, respectively.

The plane located in a different projection is found in a similar way. After that, the guiding cosines of the desired straight line are found using the normalized vector product of the perpendiculars of two intersecting planes (7), which will be the track of the particle:

$$\begin{cases} A_1 x + B_1 y + C_1 z + D_1 = 0, \\ A_2 x + B_2 y + C_2 z + D_2 = 0. \end{cases} \tag{7}$$

2.3. Muonograph construction method

The method of construction of muonographs for SSD and DTD is the same. The construction begins with the determination of the position of the triggered channels (centers of tubes or strips) during the passage of the particle and obtaining a track along the projection planes XY and XZ in the laboratory coordinate system. Next, it is necessary to find point (X_1, Y_1, Z_1) of the intersection of the track reconstructed using the projection planes with some reference plane of size Y_L and Z_L, set at a distance $X = L$ perpendicular to the axis X and passing through the studied object (Fig. 10). The geometric dimensions of the reference plane are determined by the size of the search zone in which the studied object is located.

The area of the plane, determined by the value $Y_L Z_L$, is divided into cells in increments Δy, Δz, forming a matrix M with dimension $k = \text{int}(Y_L/\Delta_y)$, $m = \text{int}(Z_L/\Delta_z)$. The number of the cells of the matrix M into which the muon track line „hits“ drawn from the detector to the plane (in the opposite direction of the track) is determined when the l-th track intersects the plane at the point with coordinates y_l and z_l. Accordingly, the unit $M[i, j] = M[i, j] + 1$ is added

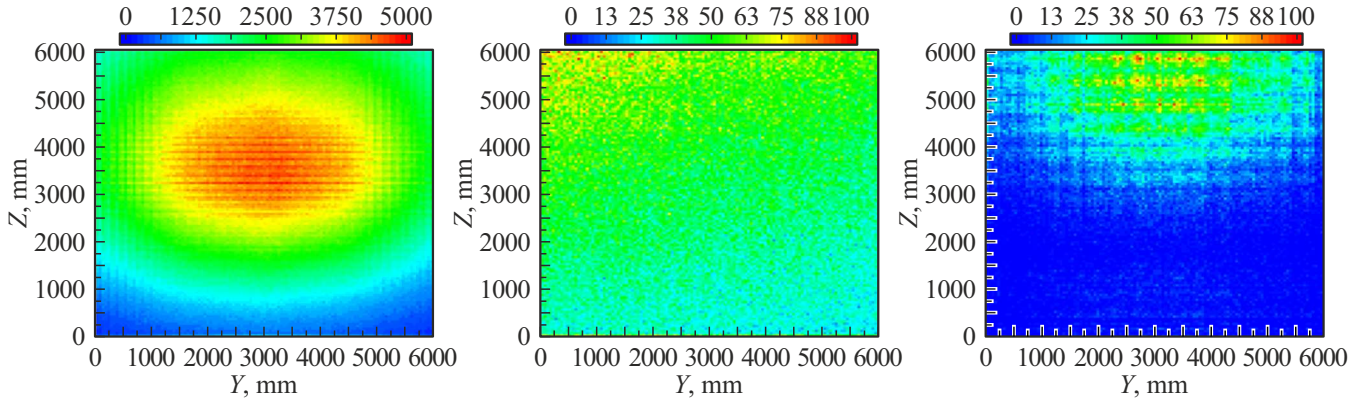

Figure 11. Base matrices: DTD at a distance of 5.3 m (left), DTD at a distance of 37.5 m (in the center) and SSD at a distance of 5.3 m (on the right).

to this cell of the matrix containing information about the number of hits of the track.

In the first approximation the coordinate resolution of the object details in the matrix M is related to the coordinate resolution of the hodoscope through the following relation:

$$\Delta Y \approx (L/b)\delta y, \quad \Delta Z \approx (L/b)\delta z, \tag{8}$$

where ΔY and ΔZ are errors in the position of the object at a distance of L from the observation point, δy and δz is the resolution of the hodoscope, b is the length of the base of the hodoscope (the distance between the extreme planes).

A difference method is used to localize regions with dynamic changes in the structure of the studied detector on the muonograph. The method is based on the subtraction of the dynamic muonograph M_{d} from the static muonograph M_{s}. At the same time, a static muonograph is formed based on the results of a long exposure, during which no dynamic changes were observed. A dynamic muonograph is obtained accordingly during the expected dynamic changes. The static muonograph is normalized to dynamic statistics. Since the distribution of the number of registered muon tracks across the matrix cells is statistical in nature, the necessary measurement accuracy can be achieved by increasing the volume of experimental data.

The values of the difference matrix M_δ are found using the formula

$$M_\delta = \frac{M_d - M_s d}{\sqrt{M_s d}}, \tag{9}$$

where d is the normalization coefficient calculated using the formula:

$$d = \frac{\sum_{i,j}(M_d[i,j])}{\sum_{i,j}(M_s[i,j])}. \tag{10}$$

For a clearer manifestation of deviations associated with dynamic changes in the structure of the object, a Gaussian low-pass filter is additionally used when subtracting matrices [22], which takes into account the weight of each cell of the matrix. The use of a low-pass Gaussian filter with a radius of R_F gives the following ratio:

$$n_{i,j} = \frac{\sum_{l,m}(f_k n_{l,m})}{\sum_{l,m}(f_k)}, \tag{11}$$

$$f_k = \exp\left(-\frac{(l-i)^2 + (m-j)^2}{2R_F^2}\right), \tag{12}$$

where $n_{i,j}$ is the value in cell (i, j) after the filter, $n_{l,m}$ is the value in cell (l, m) before filtering.

The following expressions are used for forming a smoothed difference muonograph of the deviation of the number of detected events in the cell (i, j) from the value in this cell for a static muonograph in units of statistical errors $\Delta n_{i,j}/\sigma(n_{i,j})$, taking into account the variances of the values of the cells involved in smoothing:

$$\Delta n_{i,j} = \frac{\sum_{l,m}(f_k n_{l,m})}{\sum_{l,m}(f_k)} - \frac{\sum_{l,m}(f_k \overline{n_{l,m}})}{\sum_{l,m}(f_k)}, \tag{13}$$

$$\sigma(n_{i,j}) = \frac{\sqrt{\sum_{l,m}(f_k^2 \overline{n_{l,m}})}}{\sum_{l,m}(f_k)}. \tag{14}$$

3. Muonography of lead assemblies

Experimental series of measurements on the localization of test objects (assemblies of lead bricks located at certain points within the detector aperture) were carried out to test the possibility of implementing the muonography method using a fully functional HMH prototype. The evaluation of the accuracy characteristics of the developed recording system and data processing methods was another purpose of the experiments.

Initially, an experimental series was conducted during the month-long exposure to obtain a muonograph M_{s} without test objects in the detector aperture. After the measurements were completed, test objects (lead assemblies) were sequentially installed within the aperture at different distances and heights. A new measurement was performed for

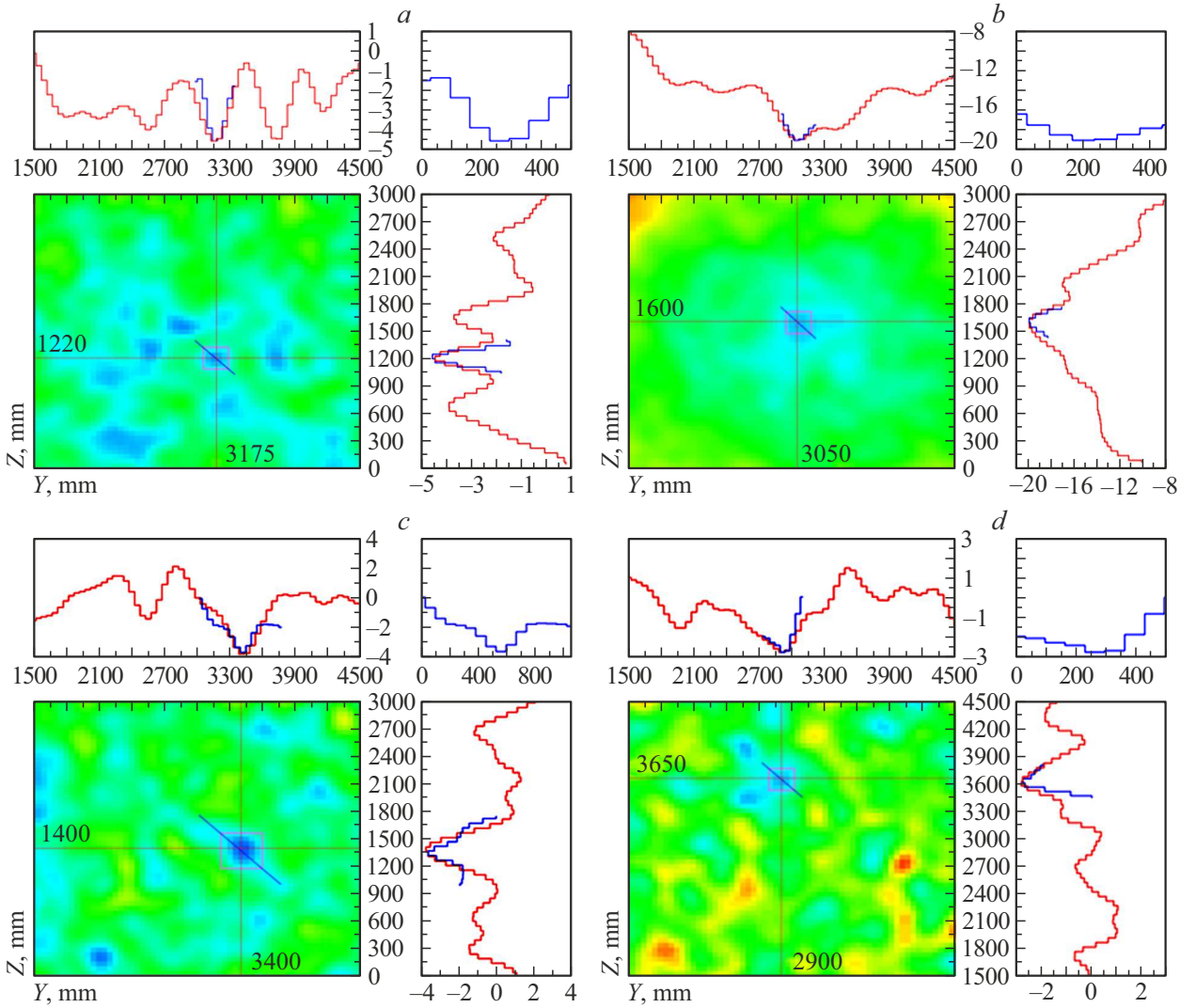

Figure 12. Difference matrices: *a* — DTD with an object at a height of 1.2 m; *b* — DTD with an object at a height of 1.6 m; *c* — DTD with an object at a height of 10.3 m; *d* — SSD with an object at a height of 1.6 m.

14 days for each position of the object and muonographs M_{d} were formed. Next, the method described in Section 2.3 was used to obtain the difference muonographs M_{δ} . Based on the analysis of muonographs M_{δ} , a conclusion was made about the coordinates and dimensions of the location of the test objects.

Several test objects were used during the experiment: an assembly of lead bricks with dimensions $200 \times 200 \times 205$ mm (placed directly opposite the detector at heights 1.2 and 1.6 m at a distance of 5.3 m from its center) and a lead brick assembly with a size of $400 \times 400 \times 430$ mm (placed on the third floor of a neighboring building at a height of 10.3 m at a distance of 37.5 m at an azimuthal angle of 17°).

Figure 11 shows the basic matrices with cells 50×50 mm, obtained using DTD and SSD data. The different intensity of the points in the matrix field indicates the spatial and angular distribution of the reconstructed muon tracks (in pieces). A mesh structure can be seen, which is attributable to the presence of gaps between the strips of a single-layer coordinate plane structure.

Fig. 12, *a, b* show the difference muonographs obtained using the DTD data in case of the localization of the first test object at heights of 1.2 and 1.6 m and a horizontal distance of 5.3 m from the center of the HMG prototype. Fig. 12, *c* shows the difference muonograph obtained using the DTD data for the second object located at a height of 10.3 m and at a distance of 37.5 m. The respective muonograph for the first object at a height of 1.6 m obtained using the SSD data is shown in Fig. 12, *d*. The following figures additionally show charts with histograms of sections along the horizontal and vertical red lines and the diagonal blue line. The regions with blue color in difference matrices correspond to a lack of events in the angular distribution of muons, the red - regions correspond to the excess of events. The squares indicate the expected size and location of the sought object.

Results of measurements of the dimensions of test objects

№ No.	Parameter (coordinates)	Actual size, mm	Measured size, mm	Absolute error size, mm	Actual position, mm	Measured position, mm	Absolute error position, mm
1	Width (Y) Height (Z)	200 205	192.1 197.7	−7.8 −7.2	3156 1203	3162.6 1214.8	6.6 11.8
2	Width (Y) Height (Z)	200 205	203.4 206.7	3.4 1.7	3052 1601	3051.3 1563.1	−0.6 −37.8
3	Width (Y) Height (Z)	400 430	345.8 460.6	−54.1 30.6	3386 1468	3416.5 1382.3	30.5 −85.6

A Gaussian low-pass filter, which takes into account the weight of each matrix cell, was additionally applied to better demonstrate deviations during matrix subtraction.

As can be seen, there are several areas with a lack of events on the obtained difference matrices. This is attributable to various fluctuations of the recorded data and their low statistical power, as a result of which various changes in the particle flow and detector operation affect the final result. The spot of the sought object is distinguished from the other (false) spots by moving the reference plane along the axis X_{Lab} near the sought object. In this case, the spots caused by statistical fluctuations change and move more strongly than a spot with the sought object, which is practically stable. In this case, the deviation value is used as a quantitative estimate, which in the case of fluctuations (false spots) changes more strongly than in the sought object.

The accuracy of localization and the size of the observed object were estimated using the histograms of the difference matrix, which are shown in the table. The average deviations of dimensions according to the measured data were ± 10 mm at a distance of 5.3 m from the detector and ± 100 mm at a distance of 37.5 m. The estimated angular accuracy of the detector based on the obtained results is ~ 2 mrad.

Conclusion

A modular design for detecting and recording systems was implemented in the prototype of a hybrid muon hodoscope developed at National Research Nuclear University MEPhI, which was later used to create a full-size wide-aperture precision hybrid muon hodoscope.

The first results confirming the performance of the developed hybrid muon hodoscope systems and the possibility of obtaining muonographs based on it were obtained based on the results of experimental series of measurements. A difference method for constructing muonographs was developed based on the results of processing experimental data on both detectors for identifying objects located at different distances and heights relative to the center of the detecting system. The limited statistics of the dynamic muonograph turned out to be the main problem of the method which led to statistical fluctuations in the finite difference muonograph and complicated the detection of the real position of the muon deficiency region associated with the presence of a test object. Despite this, the muonographs of lead brick assemblies were obtained using the data of both detectors and the analysis of these muonographs made it possible to determine their size and position in space, as well as to evaluate the localization accuracy.

Acknowledgments

The authors would like to thank the team of the Scientific & Educational Centre NEVOD (National Research Nuclear University MEPhI) for their assistance in carrying out work on the creation of a muon hodoscope, as well as the team of IRT-2000 (National Research Nuclear University MEPhI) for the opportunity to conduct an experiment with lead assemblies.

Funding

The development and study of the hybrid muon hodoscope were carried out under the scope of the agreements between the National Research Nuclear University „MEPhI“ and JSC „All-Russian Research Institute for the Operation of Nuclear Power Plants“ dated 19.11.2019 № 00-3-700-0650 and JSC „All-Russian Research Institute for the Operation of Nuclear Power Plants“ with JSC „Science and Innovation“ dated 09.04.2019 № 313/1658-D.

Conflict of interest

The authors declare that they have no conflict of interest.

References

[1] A. Simpson, A. Clarkson, S. Gardner, R.A. Jebali, R. Kaiser, D. Mahon, J. Roe, M. Ryan, C. Shearer, G. Yang. Appl. Radiat. Isot., **157**, 109033 (2020). DOI: 10.1016/j.apradiso.2019.109033

[2] C. Park, K.B. Kim, Y.S. Chung, M.K. Baek, I. Kang, S. Lee, H. Chung, Y.H. Chung. Nucl. Instrum. Methods A, **1040**, 167081 (2022). DOI: 10.1016/j.nima.2022.167081
[3] J. Saraiva, C. Alemparte, D. Belver, A. Blanco, J. Callon, J. Collazo, A. Iglesias, L. Lopes. Nucl. Instrum. Methods A, **1050**, 168183 (2023). DOI: 10.1016/j.nima.2023.168183
[4] H.S. Barbashina, V.V. Borog, R.P. Kokoulin, K.G. Companyets, A.A. Petrukhin, D.A. Timashkov, V.V. Shutenko, I.I. Yashin. *Method and apparatus for obtaining muonographs* (Patent RU2406919C2 dated 20.12.2010, Federal Institute of Industrial Property, URL: https://patentimages.storage.googleapis.com/4e/6d/b5/12929dad5e5150/RU2406919C2.pdf)
[5] I.I. Astapov, M.M. Kaverznev, Y.N. Konev, A.A. Petrukhin, S.S. Khokhlov, I.I. Yashin. *Muon hodoscope and device for diagnostics of objects* (Patent RU2761333C1 dated 07.12.2021 Federal Institute of Industrial Property, URL: https://www1.fips.ru/ofpstorage/Doc/IZPM/RUNWC1/000/000/002/761/333/%D0%98%D0%97-02761333-00001/document.pdf)
[6] I.I. Yashin, N.N. Davidenko, A.O. Dovgopoly, R.M. Fakhroutdinov, M.M. Kaverznev, K.G. Kompaniets, Yu.N. Konev, A.S. Kozhin, E.N. Paramoshkina, N.A. Pasyuk, M.Yu. Tselinenko, O.P. Yuschenko, O.V. Zolotareva. Phys. Atom. Nucl., **84**, 1171 (2021). DOI: 10.1134/S1063778821130421
[7] I.I. Yashin, V.V. Kindin, K.G. Kompaniets, N.N. Pasyuk, M.Yu. Tselinenko. Bull. Russ. Academ. Sci.: Phys., **85**, 458 (2021). DOI: 10.3103/S1062873821040389
[8] A.A. Borisov, M.Yu. Bogolyubsky, N.I. Bozhko, A.N. Isaev, A.S. Kozhin, A.V. Kozelov, I.S. Plotnikov, V.A. Senko, M.M. Soldatov, R.M. Fakhrutdinov, N.A. Shalanda, O.P. Yushchenko, V.I. Yakimchuk. PTE, **2**, 5 (2012) (in Russian).
[9] N.A. Pasyuk, K.G. Companyets, A.A. Petrukhin, M.Yu. Tselinenko, V.V. Shutenko, I.I. Yashin. PTE: accepted for publication on 06.12.2023. DOI: 10.13140/RG.2.2.21424.53762 (preprint).
[10] Website of LLC „Uniplast“, URL: http://www.uniplast-vladimir.com
[11] KURARAY's website, URL: http://kuraraypsf.jp/psf/ws.html
[12] Datasheet HAMAMATSU MPPC S13360 series — Cat. No. KAPD1052E04 Aug. 2016 DN.
[13] Company website Weeroc, URL: https://www.weeroc.com/products/sipm-read-out/petiroc-2a
[14] Company website Terasic, URL: https://www.terasic.com.tw/en/
[15] N.A. Pasyuk, A.A. Borisov, K.G. Companyets, A.S. Kozhin, R.M. Fakhrutdinov, M.Yu. Tselinenko, V.V. Shutenko, I.I. Yashin. PTE: accepted for publication on 14.08.2023. DOI: 10.13140/RG.2.2.15552.51200(preprint).
[16] N.I. Bozhko, A.N. Isaev, A.S. Kozhin, I.S. Plotnikov, V.I. Senko, M.M. Soldatov, N.A. Shalanda, V.I. Yakimchuk. *Sistema nakamernoj elektroniki na osnove modulya MT-48 dlya bestriggernogo rezhima raboty tomografa na kosmicheskih myuonakh* (IHEP Preprint 2015−13. Protvino, 2015) (in Russian).
[17] J. Bensinger, N. Bojko, A. Borisov, R. Fakhroutdinov, S. Goryatchev, V. Goryatchev, V. Gushchin, K. Hashemi, A. Kojine, A. Kononov, A. Larionov, E. Paramoshkina, A. Pilaev, N. Skvorodnev, A. Tchougouev, H. Wellenstein. Nucl. Instrum. Methods A, **494**, 480 (2002). https://doi.org/10.1016/S0168-9002(02)01535-8 A.
[18] A. Borisov, R. Fakhroutdinov, A. Kojine, A. Larionov, A. Pilaev, V. Rybatchenko, Yu. Salomatin. Nucl. Instrum. Methods A, **494**, 214 (2002). DOI: 10.1016/S0168-9002(02)01468-7
[19] G.F. Laptev. *Elementy vektornogo ischisleniya* (Nauka, M., 1975), s. 38 (in Russian).
[20] A.S. Hassanein, S. Mohammad, M. Sameer, M.E. Ragab. IJCSI, **12** (1), 139 (2015). DOI: 10.48550/arXiv.1502.02160
[21] K. Madsen, H.B. Nielsen, O. Tingleff. *Methods for Non-Linear Least Squares Problems* (IMM, DTU, Lyngby, 2004)
[22] R. Gonzalez, R. Wood, S. Eddins. *Tsifrovaya obrabotka izobrazheniy* (Tekhnosfera, M., 2012), s. 329 (in Russian).

Translated by A.Akhtyamov